Sediment dynamics control transient fluvial incision - Comparison of sediment conservation schemes in models of bedrock-alluvial river channel evolution

Jingtao Lai[1], Kimberly Huppert[1,2], and Jean Braun[1,3]

[1]Earth Surface Process Modelling, GFZ German Research Centre for Geosciences, 14473 Potsdam, Germany
[2]Department of Earth & Atmospheric Sciences, City College of New York, NY 10031, USA
[3]Institute of Earth and Environmental Sciences, University of Potsdam, 14476 Potsdam, Germany

Key Points:

- We compare two sediment conservation schemes for mixed bedrock-alluvial rivers.
- The two sediment conservation schemes predict distinct responses of the topography and sediment layer to changes in sediment supply.
- The erosion-deposition scheme with short sediment transport length scales mimics the Exner-type scheme.

Corresponding author: Jingtao Lai, `lai@gfz-potsdam.de`

Abstract

In mountain rivers, sediment from landslides or debris flows can alluviate portions or even full reaches of bedrock channel beds, influencing bedrock river incision rates. Various landscape evolution models have been developed to account for the coevolution of alluvial cover and sediment-flux-dependent bedrock incision. Despite the commonality of their aims, one major difference between these models is the way they account for and conserve sediment. We combine two of the most widely used sediment conservation schemes, an Exner-type scheme and an erosion-deposition scheme, with the saltation-abrasion model for bedrock incision to simulate the coevolution of sediment transport and bedrock incision in a mixed bedrock-alluvial river. We compare models incorporating each of these schemes and perform numerical simulations to explore the transient evolution of bedrock incision rates in response to changes in sediment input. Our results show that the time required for bedrock incision rates to reach a time-invariant value in response to changes in sediment supply is over an order of magnitude faster using the Exner-type scheme than the erosion-deposition scheme. These different response times lead to significantly different time-averaged bedrock incision rates, particularly when the sediment supply is periodic. We explore the implications of different model predictions for modeling mixed bedrock-alluvial rivers where sediment is inevitably delivered to rivers episodically during specific tectonic and climatic events.

Plain Language Summary

In places with frequent earthquakes and heavy rain, landslides often dump a lot of sand and small rocks into rivers, which can significantly impact how a river carves valleys and changes the landscape over time. Scientists have built different computer models to mimic how rivers move sand and small rocks and how this sediment can either cover and protect the underlying rock or bang against it and erode it. We compare the two most commonly used models for sediment transport to see how their predictions of long-term valley carving differ. We found that, even though the two models aim to mimic the same scenarios, they predict that river valleys will erode at much different speeds when earthquakes or landslides occasionally dump in sediment. These results guide scientists to validate and improve models for natural rivers.

1 Introduction

Rivers control the pace and style of landscape evolution in unglaciated mountain ranges (Gilbert, 1877; Whipple & Tucker, 1999). Understanding patterns of erosion and sediment transport in rivers is critical for ecosystem management (e.g., Wohl et al., 2015) and natural hazard assessment (e.g., Merz et al., 2014), yet the ways in which sediment is transported, deposited, and abraded against steep mountain river beds is not well understood. In end member cases, rivers either erode through bedrock and evacuate all sediment produced by erosion (e.g., Howard, 1994; Whipple & Tucker, 1999), or they completely alluviate their beds and transport, deposit, and rework sediment to shape their form (e.g., Willgoose et al., 1991). Most river evolution modeling has focused on these end-member cases even though most natural rivers consist of a patchwork of bare bedrock channel beds and alluviated reaches.

In these mixed bedrock-alluvial channels, the interplay between sediment transport and bedrock incision can be complex because sediment can either enhance fluvial incision by providing tools to impact and abrade bedrock, or it can protect bedrock from incision by covering the river bed (Gilbert, 1877; Sklar & Dietrich, 2001). Because of the "tool and cover" effect, an input of sediment to a channel can have complicated effects on bedrock incision. Considering even an idealized scenario of a bare bedrock channel reach downstream of a landslide (Fig. 1a), the evolution of bedrock incision rates may vary over time as this pulse of sediment is deposited and transported through the reach. Bedrock incision may initially be tool-dominated because the sediment is not thick enough to armor the river bed (Fig. 1b). The influx of sediment will thus initially provide tools to abrade the river bed and increase the incision rate (Fig. 1e). However, sediment can build up and armor the bed, and bedrock incision can become cover-dominated (Fig. 1c), with bedrock incision rates decreasing over time (Fig. 1e). Bedrock river incision may eventually cease if this sediment becomes sufficiently thick to fully cover the river bed (Fig. 1d and e).

The trajectory of river incision in response to an input of sediment depends on the amount of sediment supplied to a channel relative to its ability to transport away this sediment. If the upstream sediment flux is higher than the transport capacity of a channel reach, the reach will become fully alluviated, with bedrock incision rates evolving through all three stages of tool-dominated, cover-dominated, and fully covered behavior. We refer to this condition as "over-capacity". On the other hand, if the upstream sediment flux is lower than the transport capacity, a channel reach will become only partially armored by a dynamic sediment layer (Turowski et al., 2007). We refer to this case as "under-capacity". In this case, bedrock river incision rates still change over time, but tend towards a steady-state condition that depends on the extent to which the transport capacity exceeds the input sediment flux. If transport capacity greatly exceeds the sediment flux, the reach remains minimally covered and bedrock river incision rates tend toward a stable, time-invariant condition in which they are tools-dominated. Conversely, if the transport capacity is only slightly greater than the sediment flux, the reach will become more alluviated, with incision rates tending towards a cover-dominated condition.

In each of these cases, the timescale over which bedrock incision rates tend toward a steady, time-invariant value differs (Fig. 1e). This response time describes how fast the bedrock incision rate stabilizes following a change in sediment input. Characterizing the response time has important implications for understanding the impact of variable sediment supply on bedrock incision in mountain ranges.

Various landscape evolution models have been developed to account for the "tool and cover" effect of sediment on fluvial incision (Gasparini et al., 2007; Shobe et al., 2017; Sklar & Dietrich, 2004; Turowski et al., 2007; Zhang et al., 2015). Early models captured this nonlinear dependence of bedrock incision on sediment flux, but lacked explicit treatment of sediment dynamics (e.g., Gasparini et al., 2007; Sklar & Dietrich, 2004), making them poorly suited for simulating fluvial response to a sudden influx of sediment. More recent landscape evolution models have incorporated sediment dynamics explicitly and simulate the simultaneous evolution of sediment and bedrock layers (e.g., Campforts et al., 2020; Lague, 2010; Shobe et al., 2017; Zhang et al., 2015, 2018). Despite their common aims, these models use different governing equations and numerical schemes for simulating sediment transport and deposition. This not only affects the sediment dynamics that emerge within the models, but it likely also leads to different predictions for the evolution of the underlying bedrock and fluvial topography. However, because these schemes for simulating sediment transport and deposition have not been systematically compared, it remains unclear to what extent their predictions differ and how confidently we can characterize and forecast how a river will respond to an influx of sediment.

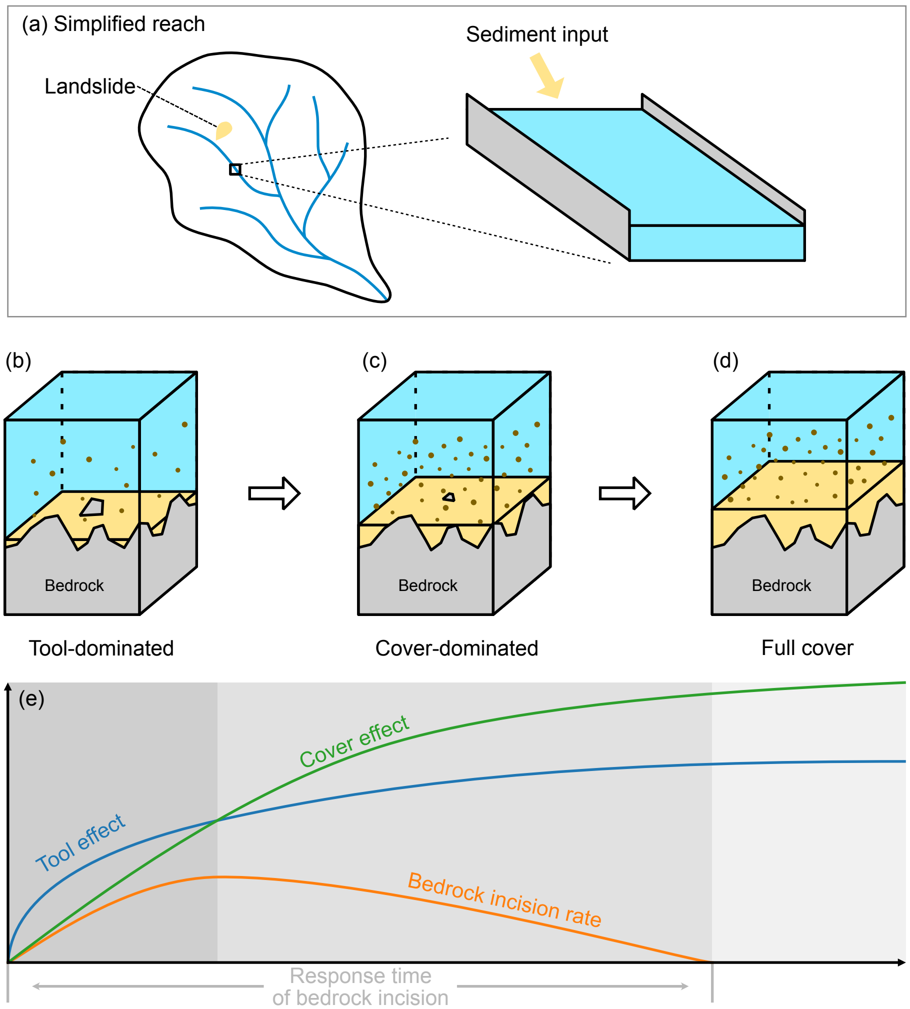

Figure 1. Cartoon illustration of (a) a simplified reach and three stages of the transient response of the reach to sudden input of sediments: (b) the tool-dominated stage, (c) the cover-dominated stage, (d) the full cover stage. Panel (e) shows the expected evolution of tool and cover effect and bedrock incision rates

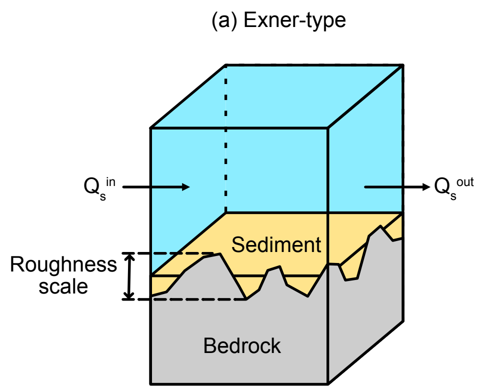

Figure 2. Cartoon illustration of the approach to sediment conservation in (a) the Exner-type scheme and (b) the erosion-deposition scheme.

In this paper, we compare the two most widely used schemes for sediment conservation in bedrock-alluvial channels: 1) an Exner-type scheme and 2) an erosion-deposition scheme. We combine them with a sediment-dependent bedrock incision model and explore the differences and similarities in the fluvial responses they predict to changes in sediment input.

2 Model description

In this section, we first describe the two approaches for sediment conservation and then describe the methods for sediment-flux-dependent bedrock incision.

2.1 Exner-type scheme

The Exner equation is a widely used equation for sediment conservation in rivers (Exner, 1925; Paola & Voller, 2005). In the Exner equation, the change rate of sediment thickness is determined by the divergence of sediment flux, which is often replaced by the divergence in sediment transport capacity in landscape evolution models (e.g., Whipple & Tucker, 2002). Sediment thickness increases when the transport capacity decreases along the flow direction, causing sediment to drop out of the water flow. Conversely, sediment thickness decreases when transport capacity increases downstream and sediment is entrained in the water flow (Fig. 2b).

The Exner equation states the change of sediment thickness H [L] over time t [T] is controlled by the change of sediment flux per unit width q_s [L^2T^{-1}] along the river:

$$(1-\phi)\frac{\partial H}{\partial t} = -\frac{\partial q_s}{\partial x} + \sigma \tag{1}$$

where ϕ is sediment porosity [ ] and σ [LT^{-1}] denotes the change of elevation per unit time by additional sediment input. In a mixed bedrock-alluvial river, additional sediment is supplied from erosion of bedrock and external sediment input (for example, landslides):

$$\sigma = (1-F_r)E_r + \frac{I_s}{W} \tag{2}$$

where E_r [LT^{-1}] is the bedrock incision rate, F_r [ ] is the fraction of eroded material entrained in the flow and carried away as suspended sediments, I_s [L^2T^{-1}] is the volumetric sediment input rate per unit length, and W [L] is the channel width.

In a mixed bedrock-alluvial river, sediment tends to accumulate in topographic lows in the riverbed (Fig. 1b), and the rate of thickness change depends on the fraction of sediment cover (Zhang et al., 2015; Shobe et al., 2017). Zhang et al. (2015) adapted this idea and introduced a cover factor p [ ] that describes the areal fraction of sediment cover into the Exner equation:

$$(1-\phi)p\frac{\partial H}{\partial t} = -\frac{\partial q_s}{\partial x} + (1-F_r)E_r + \frac{I_s}{W} \tag{3}$$

Setting all else constant, less cover of the river bed (smaller p) will result in a faster rate of sediment thickness change $\partial H/\partial t$. Conceptually, this means sediment thickness change only occurs in small areas in the topographic lows of riverbed (Zhang et al., 2015).

Sediment flux per unit width q_s is estimated as the product of the cover factor p and the sediment transport capacity per unit width q_{sc} (Chatanantavet & Parker, 2008):

$$q_s = pq_{sc} \tag{4}$$

Sediment transport capacity q_{sc} is calculated here using the Meyer-Peter-Müller relationship (Meyer-Peter & Müller, 1948):

$$q_{sc} \propto (\tau - \tau_c)^{3/2} \tag{5}$$

where τ [$ML^{-1}T^{-2}$] is the shear stress on channel bed generated by flowing water and τ_c [$ML^{-1}T^{-2}$] is the threshold shear stress.

Assuming steady, uniform flow in a wide channel (flow width $\gg$ flow depth) and using the Darcy-Weisbach flow resistance equation, τ can be written as function of the water discharge per unit width q [$\mathrm{L^2T^{-1}}$] and channel slope S [ ] (Gasparini et al., 2007; Tucker, 2004):

$$\tau \propto q^{2/3} S^{2/3} \tag{6}$$

For simplicity, we omit the threshold term, and therefore,

$$q_{sc} = K_{sc} q S \tag{7}$$

where K_{sc} [ ] is a dimensionless sediment capacity coefficient that depends on sediment density and the roughness of the channel bed (Gasparini et al., 2007; Tucker, 2004).

2.2 Erosion-deposition scheme

An alternative view of sediment conservation is based on the idea that sediment thickness is determined by the competition between sediment production (i.e., bedrock erosion) and deposition (Einstein, 1950; Kooi & Beaumont, 1994; Davy & Lague, 2009; An et al., 2018; Shobe et al., 2017). This type of model is also referred as the $\xi - q$ model (Davy & Lague, 2009; Braun, 2022) or the entrainment form of the Exner equation (An et al., 2018). We will refer this model as the erosion-deposition model following Shobe et al. (2017).

In the erosion-deposition scheme, the sediment entrainment rate E_s [$\mathrm{LT^{-1}}$] and deposition rate D_s [$\mathrm{LT^{-1}}$] are calculated explicitly, and the change of sediment thickness is:

$$(1-\phi) p \frac{\partial H}{\partial t} = D_s - E_s \tag{8}$$

The sediment entrainment rate can be written as a function of the shear stress τ (Howard, 1994; Tucker, 2004; Whipple & Tucker, 1999):

$$E_s \propto (\tau - \tau_c)^a p \tag{9}$$

where p is a cover factor that reflects the proportion of the energy used to move sediments, and it is the same p as in the Exner-type scheme. For consistency, we use the same expression for τ and omit the threshold term, as in the Exner-type model. Therefore, the sediment entrainment rate is

$$E_s \propto \left(q^{2/3} S^{2/3}\right)^a p \tag{10}$$

The value of the exponent a reflects the mechanism of particle entrainment (Whipple & Tucker, 1999; Whipple et al., 2000). For simplicity, we use $a = 3/2$ so that E_s linearly depends on q and S:

$$E_s = K_s q S p \tag{11}$$

where K_s [L^{-1}] is a sediment entrainment coefficient.

Sediment deposition rate is calculated using sediment concentration in the water (q_s/q) and sediment particle settling velocity V [LT^{-1}] (Davy & Lague, 2009; Shobe et al., 2017):

$$D_s = \frac{q_s}{q} V \tag{12}$$

Following Davy and Lague (2009), we can define $\xi = q/V$ [L] as a length scale that represents the characteristic travel distance of sediment grains before they are deposited. The length scale ξ is a key parameter that determines the behavior of the erosion-deposition model (Davy & Lague, 2009; Braun, 2022).

In the erosion-deposition model, the sediment transport capacity q_{sc} is not explicitly prescribed nor computed. When $q_s < q_{sc}$, net entrainment will occur, and when $q_s > q_{sc}$, net deposition will occur. Therefore, we can define the transport capacity as the sediment flux that results in a balance between entrainment and deposition (Davy & Lague, 2009), i.e.,

$$K_s q S p = \frac{q_{sc}}{q} V \tag{13}$$

Meanwhile, the cover factor p is 1 at transport capacity, and therefore

$$q_{sc} = K_s^* q S \tag{14}$$

where K_s^* [ ] is a dimensionless parameter defined as

$$K_s^* = \frac{K_s q}{V} = K_s \xi \tag{15}$$

reflects the competition between sediment entrainment and deposition (Shobe et al., 2017). We refer to K_s^* as the sediment transport coefficient since it is equivalent to K_{sc} in Eq. 7.

Sediment flux per unit width q_s is calculated based on local sediment conservation:

$$\frac{\partial q_s}{\partial x} = E_s + (1 - F_r) E_r - D_s + \frac{I_s}{W} \tag{16}$$

In this work, we keep $F_r = 0$ for simplicity. If we combine the above equation with Eq. 8,

$$(1 - \phi) p \frac{\partial H}{\partial t} = -\frac{\partial q_s}{\partial x} + (1 - F_r) E_r + \frac{I_s}{W} \tag{17}$$

This expression is the same as the Exner-type equation (Eq. 3)

2.3 Bedrock incision model

We use the saltation-abrasion model to simulate fluvial incision rate E_r:

$$E_r = \beta q_s (1 - p) \tag{18}$$

where the abrasion coefficient β [L^{-1}] depends on flow conditions and the characteristic grain size of the sediment that effectively abrades the bedrock (Sklar & Dietrich, 2004). Zhang et al. (2015) calculated values of β for various flow conditions and grain sizes, and their results showed that β remains approximately constant under a wide range of conditions. Therefore, we use a constant β value in this work.

2.4 The cover factor

Following previous studies, we assume that the cover factor is related to the ratio between sediment thickness H and characteristic bedrock roughness scale H^* (Zhang et al., 2015; Shobe et al., 2017). At low H/H^*, the cover factor approaches 0 and the bedrock riverbed is exposed to erosion, while at high H/H^*, the cover factor approaches 1 and the bedrock riverbed is completely armored by sediment. We use a simple form for p following Zhang et al. (2015):

$$p = \begin{cases} \frac{H}{H^*} & 0 \leq \frac{H}{H^*} \leq 1 \\ 1 & \frac{H}{H^*} > 1 \end{cases} \tag{19}$$

3 Numerical experiments

We implemented the two sediment conservation schemes into a 1D channel profile evolution model and conducted a series of experiments to investigate the sediment dynamics and the bedrock incision rates predicted by these models. For simplicity, we considered a simplified channel reach with constant slope, channel width, and water discharge (Fig 1a). Sediment only enters the reach at its upstream end. At the downstream end, we applied a free boundary condition, allowing sediment thickness at the outlet to vary over time when it is smaller than the bedrock roughness scale. Otherwise, we prohibit the outlet sediment thickness from exceeding the bedrock roughness scale by capping its thickness at the roughness scale.

To make a meaningful comparison between the two different sediment conservation schemes, we used a combination of parameters that yielded the same sediment trans-

Table 1. Description of model parameters and values

Parameter	Description	Value	Unit
β	Abrasion coefficient	1e-6	m^{-1}
K_s	Sediment entrainment coefficient	5e-6	m^{-1}
V	Sediment settling velocity	5	$m\ yr^{-1}$
K_{sc}	Sediment capacity coefficient	1	1
q	Water discharge per unit width	1e6	$m^2\ yr^{-1}$
q_{s0}	Upstream sediment input rate	varying	$m^2\ yr^{-1}$

port capacity, i.e., $K_{sc} = K_s^*$ (as described in Eqs. 7 and 14) in each model. These parameters include the sediment capacity coefficient K_{sc} in the Exner-type scheme, the sediment entrainment coefficient K_s and the settling velocity V in the erosion-deposition scheme, and the water discharge per unit width q.

Because sediment thickness can change over much shorter timescales than the bedrock channel bed, we assumed a fixed bedrock elevation in the simulations and only calculated the potential bedrock erosion rates that should occur using the saltation-abrasion model (i.e., we neglected any influence of changes in bedrock channel bed evolution over the course of our model runs).

We conducted 3 sets of experiments to test the effect of the different sediment conservation schemes on channel evolution under three different scenarios: 1) alluviation of a bare bedrock surface under constant upstream feeding; 2) evacuation of an initial sediment layer; 3) periodic upstream feeding.

3.1 Alluviation

In the first set of experiments, we simulated the alluviation of a bare bedrock reach in response to a constant upstream sediment input. The results show distinct differences in the pace and style of alluviation between the two sediment conservation schemes. Specifically, the rate of change in sediment thickness predicted by the Exner-type scheme is two orders of magnitude faster than the rate predicted by the erosion-deposition scheme (Fig. 3). Consequently, the Exner-type scheme takes less than a year to reach a steady-

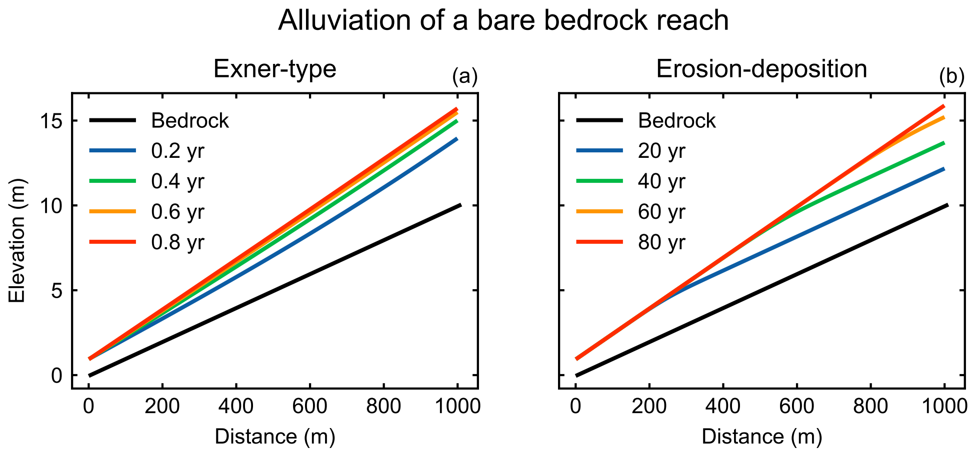

Figure 3. Alluviation of a bedrock reach predicted by models incorporating (a) the Exner-type scheme and (b) the erosion-deposition scheme. Black lines indicate the 1D profile of bedrock surface, and colored lines represent the channel elevation (fixed bedrock surface and overlying sediment) through time.

state sediment thickness (Fig. 3a), whereas the erosion-deposition scheme requires > 80 years to achieve a steady-state (Fig. 3b).

The models with different sediment conservation schemes also display different styles of alluviation. Using the Exner-type scheme, the slope increased uniformly across the entire reach, but the steepening rate declines as the channel approaches steady-state (Fig. 3a). On the contrary, using the erosion-deposition scheme, the downstream section of the channel experiences rapid steepening before the channel steepens progressively upstream at a constant rate and the entire reach attains a steady state (Fig. 3b).

Our simulations also reveal distinct trends in sediment flux, the cover factor, and consequently, bedrock incision rates predicted for each sediment conservation scheme over the course of our simulations. In Fig. 4, we illustrate the evolution of these three variables at the middle of the reach in two scenarios: 1) an over-capacity scenario in which the sediment input rate is larger than the transport capacity of the bedrock reach so that a sediment pile can form, and 2) an under-capacity scenario where the sediment feeding rate is smaller than the transport capacity and allows only partial cover.

In the over-capacity case (solid lines in Fig. 4), using the Exner-type scheme, the mid-channel sediment flux rises to the value of the upstream feeding rate slowly (in months)

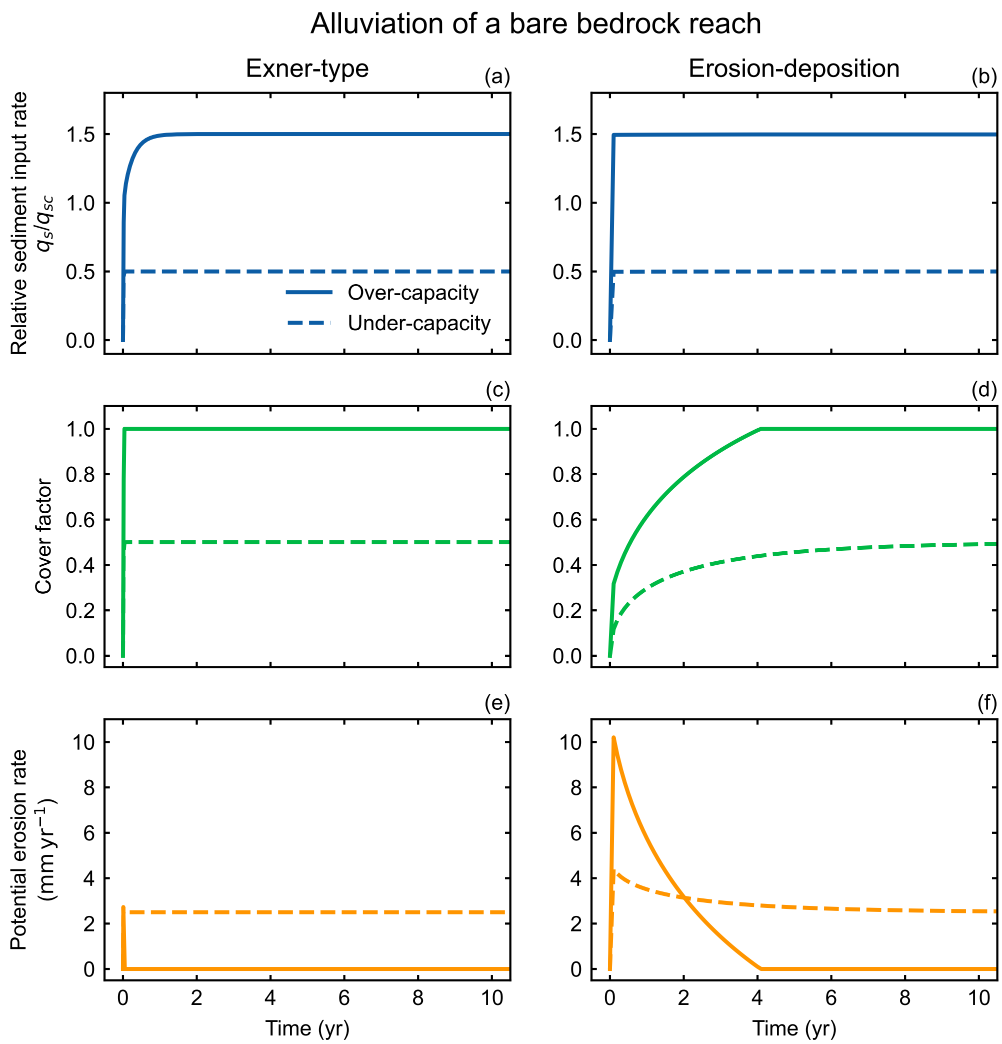

Figure 4. Evolution of (a, b) relative sediment flux, (c, d) cover factor, and (e, f) potential erosion rate during the alluviation process. The left column is the results of the Exner-type scheme, and the right column is the results of the erosion-deposition scheme. Solid lines show the results of over-capacity case, and dashed lines are results of the under-capacity case.

whereas the erosion-deposition scheme only takes a few days to adjust (solid lines in Fig. 4a and b).

In addition to sediment flux, the evolution of sediment thickness, i.e., the cover factor, is different for the two conservation schemes. Using the Exner-type scheme, the cover factor rapidly increases to 1 over a timescale of days, while the erosion-deposition scheme predicts that the cover factor increases progressively over multiple years before saturating at full cover (solid lines in Fig. 4c and d).

These different evolutionary patterns in the cover factor and sediment flux also lead to contrasting erosion rates in the two conservation schemes. Using the Exner-type scheme, because of the rapid increase of the cover factor, only a short pulse of erosion occurs before the bedrock is fully covered (solid line in Fig. 4e). On the contrary, the erosion-deposition model predicts a short tool-dominated stage in which the erosion rate increases rapidly due to the rapid rise of sediment flux, followed by a long ($\sim$ 4-year) cover-dominated stage in which the erosion rate decreases to zero as the cover factor increases (solid line in Fig. 4f). In summary, the Exner-type scheme predicts a much shorter response time of erosion rates than the erosion-deposition scheme.

In the under-capacity case where the upstream feeding rate allows only partial cover, both the Exner-type scheme and the erosion-deposition scheme predict a rapid (diurnal timescale) increase in sediment flux (dashed lines in Fig. 4a and 4b). However, there are differences in the evolution of the cover factor between the two schemes. In the Exner-type model, the cover factor increases rapidly in tandem with the increase in sediment flux (dashed line in Fig. 4c), while the erosion-deposition scheme predicts that the increase in the cover factor lags behind the sediment flux (dashed line in Fig. 4d). As a result, in the Exner-type model, the erosion rate quickly reaches steady state without a significant pulse of rapid erosion (dashed line in Fig. 4e), while the slower increase in the cover factor in the erosion-deposition model allows for a pulse of high erosion before erosion rates equilibrate to a steady-state value (dashed line in Fig. 4f).

To summarize, the erosion-deposition model predicts a slower response of the sediment cover to the upstream feeding compared to the Exner-type model. This slower response leads to a pulse of high erosion rate before the sediment cover protects the bedrock from erosion.

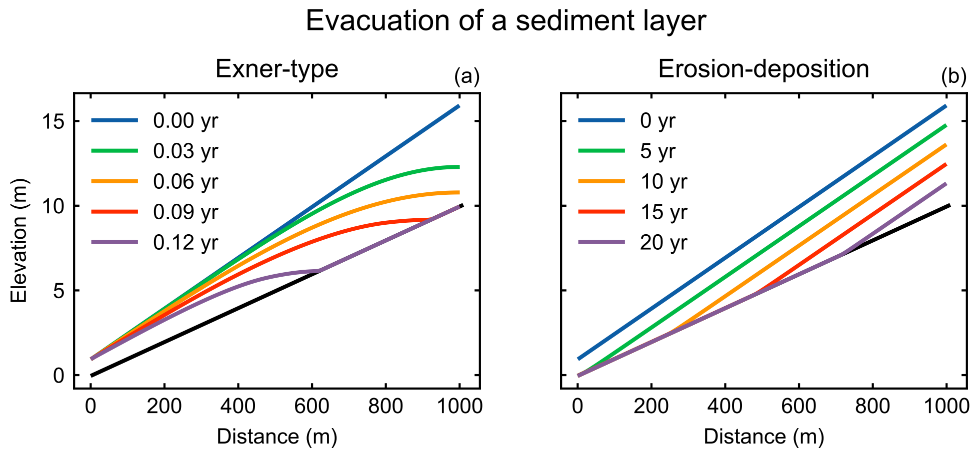

Figure 5. Evacuation of a sediment layer predicted by (a) the Exner-type scheme and (b) the erosion-deposition scheme. The initial sediment layer is created by running the model with over-capacity sediment input until the sediment thickness is in steady state. Black lines indicate the 1D profile of the bedrock surface, and colored lines represent the profiles of the surface of the sediment layer at different times.

3.2 Evacuation

In the second set of experiments, we explore the evolution of sediment flux, the cover factor, and erosion rates during the evacuation of an initial sediment layer. The initial condition is established by running the model with constant upstream sediment input until time-invariant sediment thickness is formed. We then simulate the evacuation of the sediment layer by turning off the upstream sediment input.

The rate of evacuation in the Exner-type model is 2 orders of magnitude faster than the rate in the erosion-deposition model (Fig. 5). Moreover, the two schemes predict distinct evolution styles. The Exner-type scheme predicts that the evacuation of the sediment layer initiates from the upstream end, resulting in a rapid decrease in sediment thickness near the upstream end of the channel (Fig. 5a). On the contrary, in the erosion-deposition model, the elevation of the sediment layer decreases uniformly along the channel, and the sediment near the downstream end of the channel is evacuated first (Fig. 5b).

In addition to different styles of evacuation, the two models also predict different evolution of sediment flux, the cover factor, and erosion rates. Similarly to the alluviation experiments, we explore an over-capacity scenario (solid lines in Fig. 6) and an under-capacity scenario (dashed lines in Fig. 6).

In the over-capacity scenario (solid lines in Fig. 6), both models predict rapid decreases of sediment flux after sediment input ceases and evacuation of the sediment begins (solid lines in Fig. 6a and b). The sediment flux drops rapidly to zero in the Exner-type model due to its faster evacuation rate (Fig. 6a). Using the erosion-deposition scheme, although the sediment flux also drops rapidly, it still remains at a very low non-zero value for $\sim$ 20 years as the sediment pile is evacuated due to the slow evacuation rate (Figs. 5b and 6b). The fast evacuation rate predicted by the Exner-type scheme also leads to a rapid drop in the cover factor (solid line in Fig. 6c). Although the decrease in the cover factor allows for more erosion to occur, the simultaneous rapid decline in sediment flux limits the availability of sediment tools for erosion, causing the erosion rate to decrease rapidly to zero in the Exner-type scheme (solid line in Fig. 6e). In contrast, using the erosion-deposition scheme, the sediment thickness decreases slowly, allowing the cover factor to remain at 1 for $\sim$ 10 years. Once the sediment thickness drops below the roughness scale, the cover factor gradually decreases to zero (solid line in Fig. 6d). This gradual decline in the cover factor, combined with a non-zero sediment flux, results in a pulse of erosion (solid line in Fig. 6f). This pulse of erosion is similar to the erosion pulse observed in the alluviation simulations.

In the under-capacity cases where the initial steady-state sediment layer only partially covers the bedrock riverbed, both the Exner-type scheme and the erosion-deposition scheme yield similar results as the full cover cases (dashed lines in Fig. 6). The Exner-type scheme predicts a rapid decline of sediment flux to zero, leading to a rapid decrease of erosion rate (dashed lines in Fig. 6a, c, and e). In contrast, using the erosion-deposition scheme, the gradual decline of the cover factor and non-zero sediment flux result in a pulse of erosion (dashed lines in Fig. 6b, d, and f).

In summary, both models show similar behaviors in the evacuation simulations as in the alluviation simulations. The Exner-type scheme predicts fast evacuation. This exposes the bedrock bed to erosion, but at the same time causes sediment flux to decline to zero rapidly, leaving no sediment tools to erode the riverbed. In contrast, in the erosion-deposition model, the slow change in sediment thickness and non-zero sediment flux during evacuation provides sufficient time with bed exposure and tools for erosion to occur.

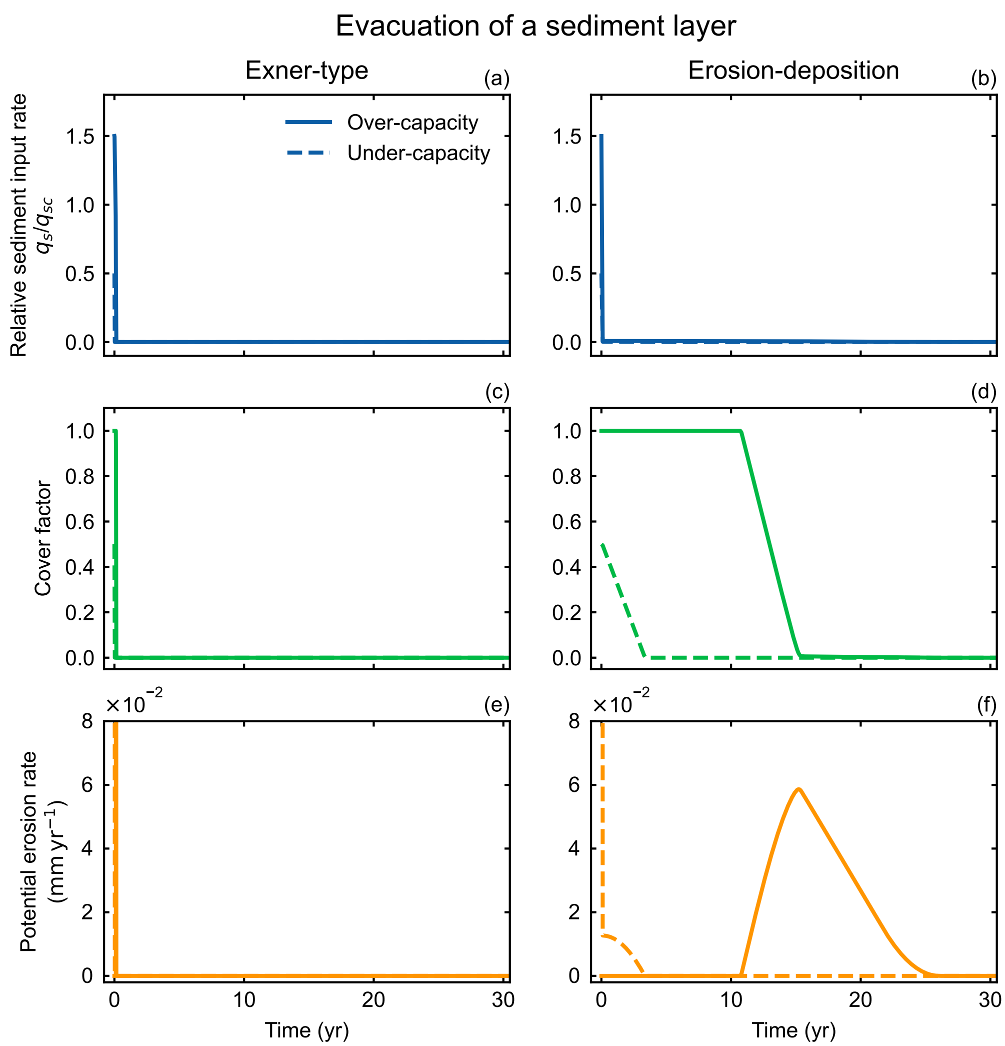

Figure 6. Evolution of (a, b) relative sediment flux, (c, d) the cover factor, and (e, f) potential erosion rate during the evacuation of an initial sediment layer. The left column is the results of the Exner-type model, and the right column is the results of the erosion-deposition model. Solid lines show the results of over-capacity case, and dashed lines are results of the under-capacity case.

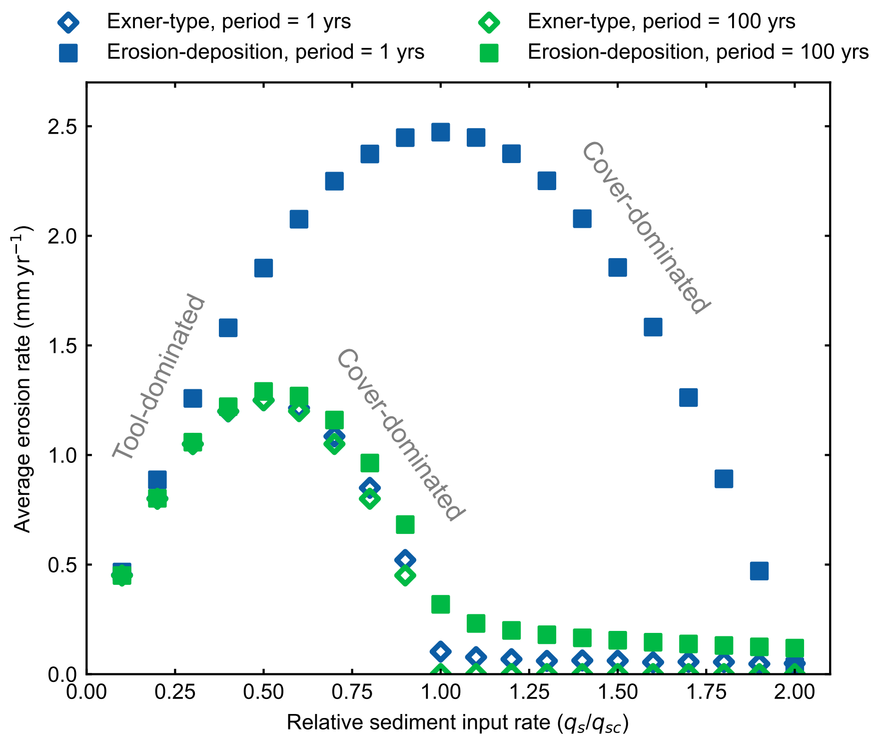

Figure 7. Time-averaged erosion rates predicted by a set of experiments with different sediment input rate and period of sediment input cycle. Open diamonds are results of Exner-type models, and solid squares are results of erosion-deposition models. Blue dots represent time-averaged erosion rates during sediment input cycles with 1-year period, and green dots represent time-averaged erosion rates during cycles with 100-year period.

3.3 Periodic sediment input

In this section, we investigate the effects of periodic sediment input on erosion rates predicted by models with Exner-type and erosion-deposition schemes. We conduct simulations with sediment input varying periodically between a feeding phase and a no-feeding phase (Fig. 8).

In this set of experiments, we vary both the period of the sediment input and the sediment input rate during the feeding phase. The river bed will be armored from erosion if the sediment input rate approaches the transport capacity of the simplified channel reach (q_s/q_{sc} approaches 1). This is indeed the case for the Exner-type scheme (open blue and green diamonds in Fig. 7): when the sediment input rate changes between different experiments, the time-averaged erosion rates are initially tool-dominated and in-

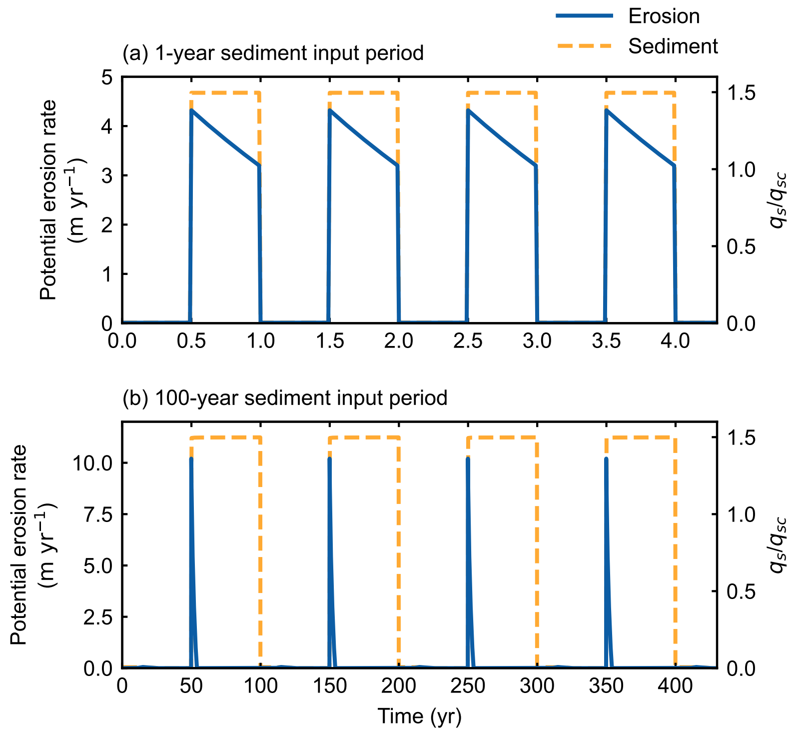

Figure 8. Evolution of potential erosion rates (solid blue lines) and sediment flux (dashed orange lines) in periodic input experiments with period of (a) 1 yr and (b) 50 yrs, using erosion-deposition model.

crease with sediment input rate. The erosion rates reach a maximum when the sediment input rate is roughly half of the sediment transport capacity ($q_s/q_{sc} \approx 0.5$). The erosion rates then become cover-dominated and decrease with increasing sediment input rate.

For the erosion-deposition scheme, the transition from the tool effect to the cover effect depends on the period of the sediment input and evacuation cycle (solid blue and green squares in Fig. 7). For long period (100 years), the transition from the tool effect to the cover effect also occurs when the sediment input rate is around half of the sediment transport capacity (solid green squares in Fig. 7). Interestingly, when the sediment input and evacuation cycle is short (1 year), the erosion rates keep increasing even if the sediment input rate is close to the transport capacity, and the transition from the tool effect to the cover effect occurs at a higher sediment input rate (solid blue squares in Fig. 7).

To understand the reason why short sediment input cycles cause the tool-cover transition to occur at a higher sediment input rate in the erosion-deposition scheme, we plot the time series of bedrock incision rates predicted by the erosion-deposition scheme in Fig. 8. Similar to the alluviation experiments (Fig. 4f), the erosion-deposition scheme predicts a pulse of erosion during the sediment feeding phase (Fig. 8). In particular, when the duration of the sediment feeding phase is shorter than the duration of the erosion pulse ($\sim$ 4 years in our simulations), erosion can occur during the entire feeding phase, even though the sediment input rate is higher than the transport capacity (Fig. 8a). On the contrary, when the duration of the feeding phase is longer than the duration of the erosion pulse, the bedrock is fully covered for most of the feeding phase and no erosion occurs (Fig. 8b). Therefore, even though the sediment input rates are the same, shorter periods of sediment input result in faster time-averaged erosion rates, causing the transitions between tool-dominated and cover-dominated behavior to occur at higher sediment input rates.

4 Discussion

4.1 Response time

Our simulations demonstrate that the erosion-deposition model predicts much longer response times of sediment thickness than the Exner-type model when there is a change of sediment flux. Because sediment thickness affects the exposure of the riverbed to erosion, characterizing the response time of sediment thickness is crucial to understand the long-term evolution of mountain ranges. We thus derive the characteristic sediment thickness response times of the two models.

We consider a simplified flat alluvial reach ($p = 1$) with constant water discharge q. For simplicity, we assume the porosity is 0 ($\phi = 0$) and neglect bedrock incision ($E_r = 0$) and additional sediment input ($I_s = 0$). We can write the evolution of sediment thickness H in Exner-type scheme as:

$$\frac{\partial H}{\partial t} = -K_{sc} q \frac{\partial^2 H}{\partial x^2} \tag{20}$$

and in erosion-deposition scheme as:

$$\frac{\partial H}{\partial t} = \frac{q_s}{q} V - K_s q \frac{\partial H}{\partial x} \tag{21}$$

In order to recover the characteristic timescales, we introduce the following dimensionless variables:

$$H' = \frac{H}{S_0 L_0},\ x' = \frac{x}{L_0},\ t' = \frac{t}{\tau} \tag{22}$$

where L_0 is the length of the channel reach, S_0 is a characteristic slope, τ is a characteristic timescale. We aim to derive τ for both Exner-type and erosion-deposition schemes.

Using the dimensionless variables, we can write the dimensionless form of Eq. 20:

$$\frac{\partial H'}{\partial t'} = -\frac{K_{sc} q \tau}{L_0^2} \frac{\partial^2 H'}{\partial x'^2} \tag{23}$$

Setting the coefficient in front of $\frac{\partial^2 H'}{\partial x'^2}$ to be unity gives the characteristic timescale for the Exner-type scheme:

$$\tau_{ex} = \frac{L_0^2}{K_{sc} q} \tag{24}$$

The characteristic timescale of the Exner-type scheme scales with the square of the characteristic length and is inversely correlated with the transport capacity coefficient K_{sc} and water flux q.

For the erosion-deposition scheme, we introduce a new dimensionless sediment flux:

$$q_s' = \frac{q_s}{K_s^* q S_0} \tag{25}$$

and therefore, the dimensionless form of Eq. 21 is

$$\frac{\partial H'}{\partial t'} = \frac{K_s^* q \tau}{L_0 \xi} (q_s' - \frac{\partial H'}{\partial x'}) \tag{26}$$

Consequently, the characteristic timescale is

$$\tau_{ed} = \frac{L_0 \xi}{K_s^* q} \tag{27}$$

To confirm the theoretical characteristic timescales are properly representative of the response times, we calculated the response time of sediment thickness in our numerical models by determining the time required for the modeled sediment layer to reach within 1% of the steady-state sediment thickness. The results show that the response times of the Exner-type scheme follow the expected theoretical characteristic timescales (purple markers and purple dashed line in Fig. 9). When the sediment transport length scale ξ exceeds the length of the simplified reach, the response times of the erosion-deposition scheme also follow the characteristic timescale, and the erosion-deposition scheme predicts longer response times than the Exner-type scheme (blue line and markers at length

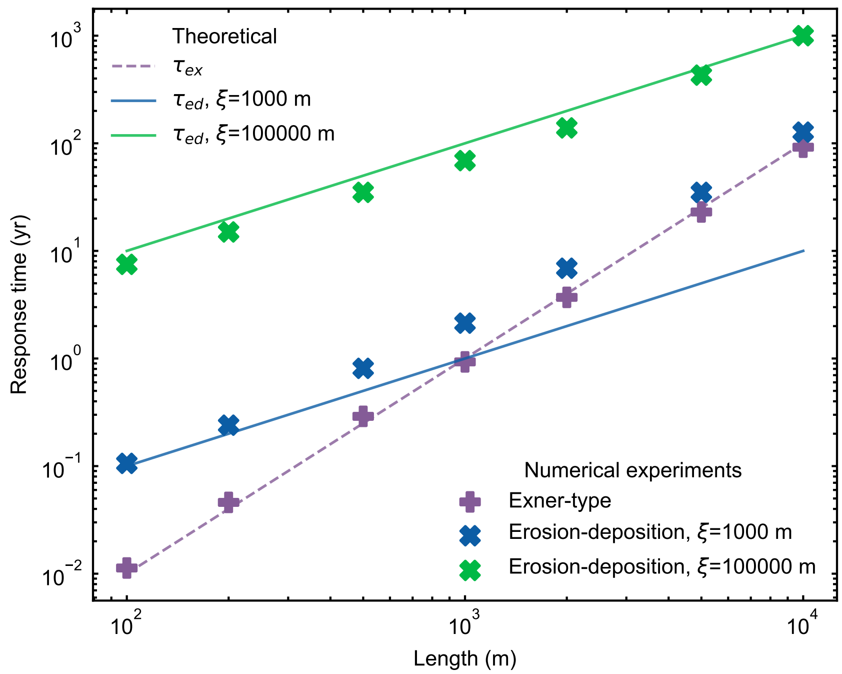

Figure 9. Theoretical characteristic timescales (lines) and simulated response times (dots) of the two schemes. Purple lines and dots are the characteristic timescales and simulated response times of the Exner-type model, respectively. Green and blue lines represent the characteristic timescales of the erosion-deposition scheme with different values of ξ, and green and blue dots show the simulated response times using the erosion-deposition scheme with different ξ values.

$< 10^3$ m and green line and markers in Fig. 9). However, if ξ is shorter than the length of the simplified reach, the characteristic timescale fails to predict the response times for the erosion-deposition scheme, and the two schemes result in similar response times that follow the characteristic timescale of the Exner-type scheme (blue and purple markers at lengths $> 10^3$ m in Fig. 9).

Our findings suggest that, when the length of the reach is greater than the characteristic sediment transport length $L_0 > \xi$, the response time of the erosion-deposition scheme approaches the response time of the Exner-type scheme. This is consistent with previous work suggesting that the behaviors of the erosion-deposition scheme with short transport length ξ approaches to behaviors of the Exner-type scheme (An et al., 2018; Braun, 2022; Davy & Lague, 2009). Davy and Lague (2009) show that the sediment flux q_s will be close to its local transport capacity when ξ is small. In such case, $q_s' \approx \frac{\partial H'}{\partial x'}$, and the characteristic timescale obtained from Eq. 26 fails to predict the response time because the left-hand side of Eq. 26 will be close to 0. Instead, we should use the sediment conservation equation in terms of sediment flux for the erosion-deposition scheme (Eq. 17):

$$\frac{\partial H}{\partial t} = -\frac{\partial q_s}{\partial x} = -\frac{\partial}{\partial x}(K_s^* q \frac{\partial H}{\partial x}) \tag{28}$$

where sediment flux is approximated using local sediment transport capacity $K_s^* q \frac{\partial H}{\partial x}$. The above equation is equivalent to the Exner-type scheme (Eq. 20) and its characteristic timescale is:

$$\tau_{ed} = \frac{L_0^2}{K_s^* q} \tag{29}$$

This equation results in the same characteristic timescale as the Exner-type scheme when the sediment transport coefficients for each scheme are equal $K_{sc} = K_s^*$, which is consistent with the observed analogous response times when $L_0 > \xi$.

When the reach is shorter than the transport length $L_0 < \xi$, the characteristic timescale of the erosion-deposition model depends linearly on the sediment transport length ξ (Eq. 27). In this case, the ratio of the characteristic timescales of the Exner-type and the erosion-deposition models is

$$\frac{\tau_{ed}}{\tau_{ex}} = \frac{K_{sc}}{K_s^*}\frac{\xi}{L_0} \tag{30}$$

Because $L_0 < \xi$, this ratio is always smaller than 1 if $K_{sc} = K_s^*$, suggesting that the Exner-type scheme always adjust more quickly than the erosion-deposition scheme when the sediment transport length scale is longer than the length of the reach.

The response time has important implications for modeling mixed bedrock-alluvial rivers in regions where landslides are a major source of sediment input to rivers (Francis et al., 2022; Hovius et al., 1997, 2000; Korup, 2005; Yanites et al., 2010). The frequency of landslide-triggering events spans from every year (e.g., rainstorms) to every 100-1000 years (for example, earthquakes; Berryman et al., 2012). Furthermore, the frequency and magnitude of landsliding may change in response to changes in climate (Handwerger et al., 2022; Gariano & Guzzetti, 2016). For example, increased air temperature in the French Alps has caused more frequent landsliding in spring (Saez et al., 2013). The changes of wildfire frequency may also have impact on the frequency of landsliding (Jackson & Roering, 2009). Our periodic sediment input experiments show that the relative duration of sediment input compared to the response time plays an important role in determining bedrock incision rates (Figs. 8 and 7). Using our analytic expressions (Eqs. 27 and 29), we calculated the characteristic timescale of the erosion-deposition scheme for different

ξ values and reach lengths, and the results show that the characteristic timescale spans from less than 1 year to over 1000 years, depending on values of ξ and lengths of the reach (blue and purple lines in Fig. 9). Therefore, the value of ξ should be chosen with caution when modeling rivers in regions where frequent landslides causes episodic sediment input to river networks since accepted values for ξ yield response times that can be shorter than, comparable to, or longer than landslide recurrence intervals, significantly affecting channel response.

4.2 The value of ξ controls the behavior of erosion-deposition scheme

Both our numerical simulations and analytical solutions show that the response time of the erosion-deposition scheme approaches the response time of the Exner-type scheme when the characteristic transport length ξ is shorter than the reach (Fig. 9). This is consistent with previous work showing that the erosion-deposition scheme behaves similarly to the Exner-type scheme for small ξ values (An et al., 2018; Davy & Lague, 2009; Shobe et al., 2017). The erosion-deposition scheme may therefore have wider applicability than the Exner-type scheme in modeling natural rivers, provided they also show a wider range of behavior. In any case, using a small ξ value in the erosion-deposition model mimics the sediment dynamics predicted by the Exner-type scheme.

However, value of ξ in natural systems remains poorly constrained. Davy and Lague (2009) calculated ξ values for different grain sizes and found that ξ values ranges from a couple of centimeters to a couple of kilometers – at least an order of magnitude smaller than in situ measurements of grain travel lengths by tracking particles in sand bed or gravel bed streams.

Yuan et al. (2019) introduced a new parameter G [ ] for the erosion-deposition model:

$$G = \frac{V}{r} \tag{31}$$

where r [LT^{-1}] is the rainfall rate. The value of ξ can be related to G if we assume channel width W [L] scales with drainage area A [L^2] (i.e., $W = k_w A^b$):

$$\xi = \frac{q}{V} = \frac{rA/W}{Gr} = \frac{A^{1-b}}{k_w G} \tag{32}$$

The value of b is typically around 0.5 and the value of k_w ranges from 0.01 to 0.001 for mountain rivers (Montgomery & Gran, 2001). Observations from experimental and natural sedimentary landscapes suggest a range of G value between 1 and 2 (Guerit et al., 2019). If we assume a value of 1 for G, the value of ξ is on the order of 100-1000 km, for catchments with sizes range from 10 to 100 km^2.

Because ξ plays a fundamental role in determining the behavior of the erosion-deposition scheme, we suggest that future research is needed to better constrain this value. Guerit et al. (2019) derived a relationship between ξ and the slopes of alluvial fans and their upstream rivers, and therefore, the value of ξ can be estimated using topographic data. More data should be collected to estimate ξ using this method. Other new datasets and techniques, such as sediment transit time estimates using cosmogenic nuclide concentrations (e.g., Repasch et al., 2020; Wittmann et al., 2011) or luminescence (e.g., Guyez et al., 2023) and datasets of "smartrock" tracer transport(e.g., Pretzlav et al., 2021), can provide additional constraints on the sediment transport dynamics in river system and shed light on the value of ξ in natural system.

5 Conclusion

We coupled two schemes for sediment conservation with sediment-flux-dependent bedrock incision to compare the transient channel response predicted by the two schemes. We find that the Exner-type scheme predicts faster response of sediment thickness than the erosion-deposition scheme, and consequently, the cover effect of sediments causes bedrock incision rates to reach time-invariant values at a faster rate using the Exner-type scheme than the erosion-deposition scheme. The different response times predicted by the two schemes lead to distinct channel response when the sediment input is periodic. In particular, in the erosion-deposition model, when the duration of the sediment feeding phase is shorter than or similar to the response time, erosion can still occur even when the sediment input rate is higher than the sediment transport capacity. This finding suggests that the response time of the sediment conservation scheme should be taken into consideration when modeling bedrock-alluvial rivers with episodic sediment input.

Our analyses show that the sediment transport length scale ξ is a critical control on the response time of the erosion-deposition scheme. Small ξ value causes the erosion-deposition scheme to yield similar response times as the Exner-type scheme. Therefore, we suggest that the erosion-deposition scheme may have wider applicability in capturing the range of fluvial responses to sediment input than the Exner-type scheme. Topographic, geochemical, and field measurements, including datasets of sediment transient time and “smartrock” tracers, may shed light on the value of ξ and help validate and improve models of mixed bedrock-alluvial channel evolution.

Open Research Section

The model and numerical experiments are archived at `https://github.com/laijingtao/model_comparison_ED_vs_Exner`.

Acknowledgments

J. Lai is supported by funding from the European Union’s Marie Skłodowska-Curie Actions Postdoctoral Fellowship No. 101064307.

References

An, C., Moodie, A. J., Ma, H., Fu, X., Zhang, Y., Naito, K., & Parker, G. (2018). Morphodynamic model of the lower Yellow River: Flux or entrainment form for sediment mass conservation? *Earth Surface Dynamics*, *6*(4), 989–1010. doi: 10.5194/esurf-6-989-2018

Berryman, K. R., Cochran, U. A., Clark, K. J., Biasi, G. P., Langridge, R. M., & Villamor, P. (2012). Major Earthquakes Occur Regularly on an Isolated Plate Boundary Fault. *Science*, *336*(6089), 1690–1693. doi: 10.1126/science.1218959

Braun, J. (2022). Comparing the transport-limited and ξ–q models for sediment transport. *Earth Surface Dynamics*, *10*(2), 301–327. doi: 10.5194/esurf-10-301-2022

Campforts, B., Shobe, C. M., Steer, P., Vanmaercke, M., Lague, D., & Braun, J. (2020). HyLands 1.0: A hybrid landscape evolution model to simulate the impact of landslides and landslide-derived sediment on landscape evolution. *Geoscientific Model Development*, *13*(9), 3863–3886. doi: 10.5194/gmd-13-3863-2020

Chatanantavet, P., & Parker, G. (2008). Experimental study of bedrock channel alluviation under varied sediment supply and hydraulic conditions. *Water Resources Research*, *44*(12), 1–19. doi: 10.1029/2007WR006581

Davy, P., & Lague, D. (2009). Fluvial erosion/transport equation of landscape evolution models revisited. *Journal of Geophysical Research*, *114*(F3), F03007. doi:

10.1029/2008JF001146

Einstein, H. A. (1950). *The bed-load function for sediment transportation in open channel flows* (No. 1026). US Department of Agriculture.

Exner, F. M. (1925). Uber die wechselwirkung zwischen wasser und geschiebe in flussen. *Akad. Wiss. Wien Math. Naturwiss. Klasse*, *134*(2a), 165–204.

Francis, O., Fan, X., Hales, T., Hobley, D., Xu, Q., & Huang, R. (2022). The Fate of Sediment After a Large Earthquake. *Journal of Geophysical Research: Earth Surface*, *127*(3), e2021JF006352. doi: 10.1029/2021JF006352

Gariano, S. L., & Guzzetti, F. (2016). Landslides in a changing climate. *Earth-Science Reviews*, *162*, 227–252. doi: 10.1016/j.earscirev.2016.08.011

Gasparini, N. M., Whipple, K. X., & Bras, R. L. (2007). Predictions of steady state and transient landscape morphology using sediment-flux-dependent river incision models. *Journal of Geophysical Research: Earth Surface*, *112*(3), 1–20. doi: 10.1029/2006JF000567

Gilbert, G. (1877). *Report on the geology of the Henry Mountains* (Tech. Rep.). Washington, D.C.: U.S. Government Printing Office. doi: 10.3133/70039916

Guerit, L., Yuan, X.-P., Carretier, S., Bonnet, S., Rohais, S., Braun, J., & Rouby, D. (2019). Fluvial landscape evolution controlled by the sediment deposition coefficient: Estimation from experimental and natural landscapes. *Geology*, *47*(9), 853–856. doi: 10.1130/G46356.1

Guyez, A., Bonnet, S., Reimann, T., Carretier, S., & Wallinga, J. (2023). A Novel Approach to Quantify Sediment Transfer and Storage in Rivers—Testing Feldspar Single-Grain pIRIR Analysis and Numerical Simulations. *Journal of Geophysical Research: Earth Surface*, *128*(2), e2022JF006727. doi: 10.1029/2022JF006727

Handwerger, A. L., Fielding, E. J., Sangha, S. S., & Bekaert, D. P. S. (2022). Landslide Sensitivity and Response to Precipitation Changes in Wet and Dry Climates. *Geophysical Research Letters*, *49*(13), e2022GL099499. doi: 10.1029/2022GL099499

Hovius, N., Stark, C. P., & Allen, P. A. (1997). Sediment flux from a mountain belt derived by landslide mapping. *Geology*, *25*(3), 231–234. doi: 10.1130/0091-7613(1997)025⟨0231:SFFAMB⟩2.3.CO;2

Hovius, N., Stark, C. P., Hao-Tsu, C., & Jiun-Chuan, L. (2000). Supply and Removal of Sediment in a Landslide-Dominated Mountain Belt: Central Range, Taiwan. *The Journal of Geology*, *108*(1), 73–89. doi: 10.1086/314387

Howard, A. D. (1994). A detachment limited model of drainage basin evolution. *Water Resources Research*, *30*(7), 2261–2285. doi: 10.1029/94WR00757

Jackson, M., & Roering, J. J. (2009). Post-fire geomorphic response in steep, forested landscapes: Oregon Coast Range, USA. *Quaternary Science Reviews*, *28*(11), 1131–1146. doi: 10.1016/j.quascirev.2008.05.003

Kooi, H., & Beaumont, C. (1994). Escarpment evolution on high-elevation rifted margins: Insights derived from a surface processes model that combines diffusion, advection, and reaction. *Journal of Geophysical Research: Solid Earth*, *99*(B6), 12191–12209. doi: 10.1029/94JB00047

Korup, O. (2005). Large landslides and their effect on sediment flux in South Westland, New Zealand. *Earth Surface Processes and Landforms*, *30*(3), 305–323. doi: 10.1002/esp.1143

Lague, D. (2010). Reduction of long-term bedrock incision efficiency by short-term alluvial cover intermittency. *Journal of Geophysical Research: Earth Surface*, *115*(F2), 1–23. doi: 10.1029/2008JF001210

Merz, B., Aerts, J., Arnbjerg-Nielsen, K., Baldi, M., Becker, A., Bichet, A., … Nied, M. (2014). Floods and climate: Emerging perspectives for flood risk assessment and management. *Natural Hazards and Earth System Sciences*, *14*(7), 1921–1942. doi: 10.5194/nhess-14-1921-2014

Meyer-Peter, E., & Müller, R. (1948). Formulas for Bed-Load transport. In *IAHSR 2nd meeting.* Stockholm.

Montgomery, D. R., & Gran, K. B. (2001). Downstream variations in the width of bedrock channels. *Water Resources Research*, *37*(6), 1841–1846. doi: 10.1029/2000WR900393

Paola, C., & Voller, V. R. (2005). A generalized Exner equation for sediment mass balance. *Journal of Geophysical Research: Earth Surface*, *110*(F4). doi: 10.1029/2004JF000274

Pretzlav, K. L. G., Johnson, J. P. L., & Bradley, D. N. (2021). Smartrock Transport From Seconds to Seasons: Shear Stress Controls on Gravel Diffusion Inferred From Hop and Rest Scaling. *Geophysical Research Letters*, *48*(9), e2020GL091991. doi: 10.1029/2020GL091991

Repasch, M., Wittmann, H., Scheingross, J. S., Sachse, D., Szupiany, R., Orfeo, O., … Hovius, N. (2020). Sediment Transit Time and Floodplain Storage Dynamics in Alluvial Rivers Revealed by Meteoric ^{10}Be. *Journal of Geophysical Research: Earth Surface*, *125*(7), e2019JF005419. doi: 10.1029/2019JF005419

Saez, J. L., Corona, C., Stoffel, M., & Berger, F. (2013). Climate change increases frequency of shallow spring landslides in the French Alps. *Geology*, *41*(5), 619–622. doi: 10.1130/G34098.1

Shobe, C. M., Tucker, G. E., & Barnhart, K. R. (2017). The SPACE 1.0 model: A Landlab component for 2-D calculation of sediment transport, bedrock erosion, and landscape evolution. *Geoscientific Model Development*, *10*(12), 4577–4604. doi: 10.5194/gmd-10-4577-2017

Sklar, L. S., & Dietrich, W. E. (2001). Sediment and rock strength controls on river incision into bedrock. *Geology*, *29*(12), 1087. doi: 10.1130/0091-7613(2001)029⟨1087:SARSCO⟩2.0.CO;2

Sklar, L. S., & Dietrich, W. E. (2004). A mechanistic model for river incision into bedrock by saltating bed load. *Water Resources Research*, *40*(6), 1–22. doi: 10.1029/2003WR002496

Tucker, G. E. (2004). Drainage basin sensitivity to tectonic and climatic forcing: Implications of a stochastic model for the role of entrainment and erosion thresholds. *Earth Surface Processes and Landforms*, *29*(2), 185–205. doi: 10.1002/esp.1020

Turowski, J. M., Lague, D., & Hovius, N. (2007). Cover effect in bedrock abrasion: A new derivation and its implications for the modeling of bedrock channel morphology. *Journal of Geophysical Research: Earth Surface*, *112*(F4). doi: 10.1029/2006JF000697

Whipple, K. X., Hancock, G. S., & Anderson, R. S. (2000). River incision into bedrock: Mechanics and relative efficacy of plucking, abrasion, and cavitation. *Geological Society of America Bulletin*, *112*(3), 490–503. doi: 10.1130/0016-7606(2000)112⟨490:RIIBMA⟩2.0.CO;2

Whipple, K. X., & Tucker, G. E. (1999). Dynamics of the stream-power river incision model: Implications for height limits of mountain ranges, landscape response timescales, and research needs. *Journal of Geophysical Research: Solid Earth*, *104*(B8), 17661–17674. doi: 10.1029/1999JB900120

Whipple, K. X., & Tucker, G. E. (2002). Implications of sediment-flux-dependent river incision models for landscape evolution. *Journal of Geophysical Research*, *107*(B2), 2039. doi: 10.1029/2000JB000044

Willgoose, G., Bras, R. L., & Rodriguez-Iturbe, I. (1991). A coupled channel network growth and hillslope evolution model: 1. Theory. *Water Resources Research*, *27*(7), 1671–1684. doi: 10.1029/91WR00935

Wittmann, H., Von Blanckenburg, F., Maurice, L., Guyot, J., & Kubik, P. (2011). Recycling of Amazon floodplain sediment quantified by cosmogenic 26Al and 10Be. *Geology*, *39*(5), 467–470. doi: 10.1130/G31829.1

Wohl, E., Bledsoe, B. P., Jacobson, R. B., Poff, N. L., Rathburn, S. L., Walters, D. M., & Wilcox, A. C. (2015). The Natural Sediment Regime in Rivers: Broadening the Foundation for Ecosystem Management. *BioScience*, *65*(4), 358–371. doi: 10.1093/biosci/biv002

Yanites, B. J., Tucker, G. E., Mueller, K. J., & Chen, Y.-G. (2010). How rivers react to large earthquakes: Evidence from central Taiwan. *Geology*, *38*(7), 639–642. doi: 10.1130/G30883.1

Yuan, X. P., Braun, J., Guerit, L., Rouby, D., & Cordonnier, G. (2019). A New Efficient Method to Solve the Stream Power Law Model Taking Into Account Sediment Deposition. *Journal of Geophysical Research: Earth Surface*, *124*(6), 1346–1365. doi: 10.1029/2018JF004867

Zhang, L., Parker, G., Stark, C. P., Inoue, T., Viparelli, E., Fu, X., & Izumi, N. (2015). Macro-roughness model of bedrock–alluvial river morphodynamics. *Earth Surface Dynamics*, *3*(1), 113–138. doi: 10.5194/esurf-3-113-2015

Zhang, L., Stark, C., Schumer, R., Kwang, J., Li, T., Fu, X., ... Parker, G. (2018). The Advective-Diffusive Morphodynamics of Mixed Bedrock-Alluvial Rivers Subjected to Spatiotemporally Varying Sediment Supply. *Journal of Geophysical Research: Earth Surface*, *123*(8), 1731–1755. doi: 10.1029/2017JF004431

Figure 1.

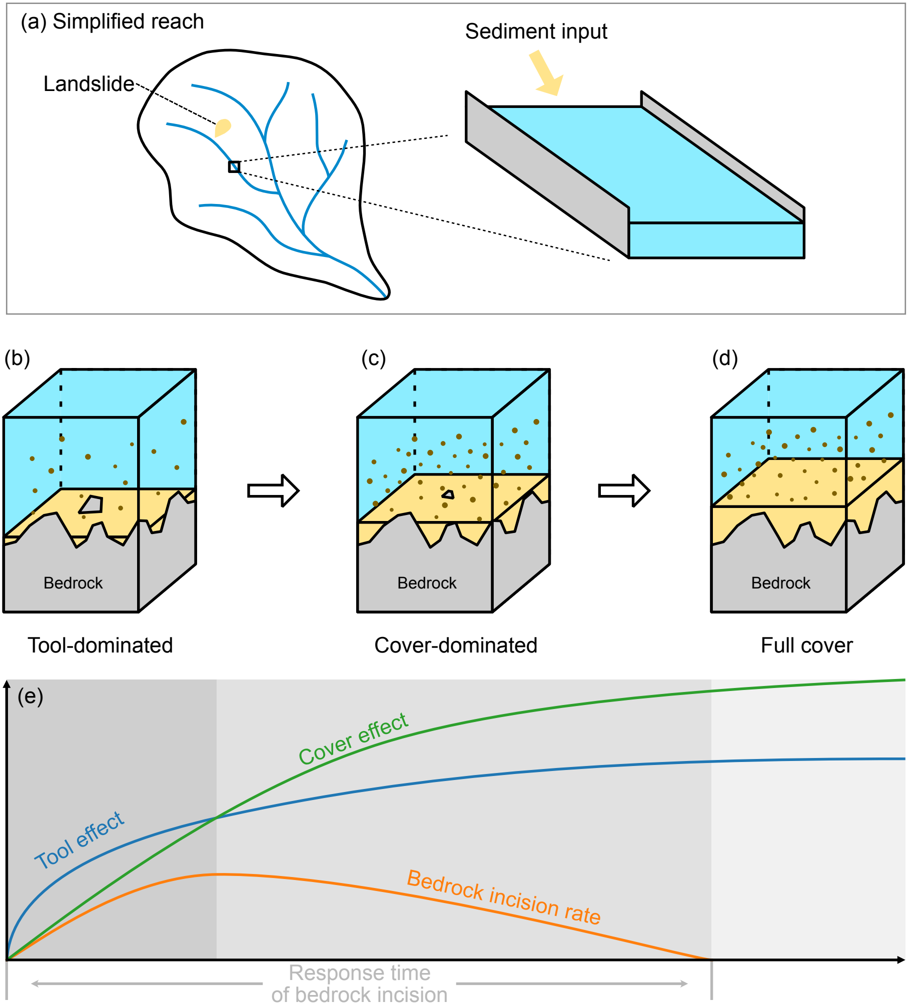
(a) Simplified reach
Landslide
Sediment input
(b)
(c)
(d)
Bedrock
Bedrock
Bedrock
Tool-dominated
Cover-dominated
Full cover
(e)
Cover effect
Tool effect
Bedrock incision rate
Response time
of bedrock incision

Figure 2.

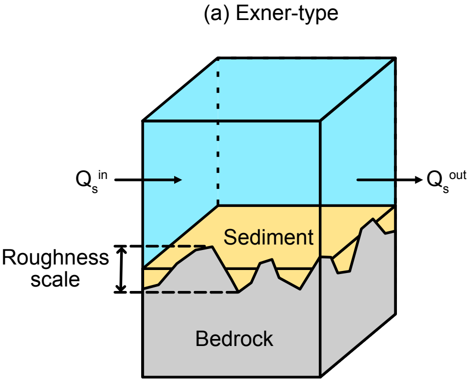

(a) Exner-type
(b) Erosion-deposition
Q_s^{in}
Q_s^{out}
Sediment
Roughness scale
Bedrock
D_s
E_s
Sediment
Bedrock

Figure 3.

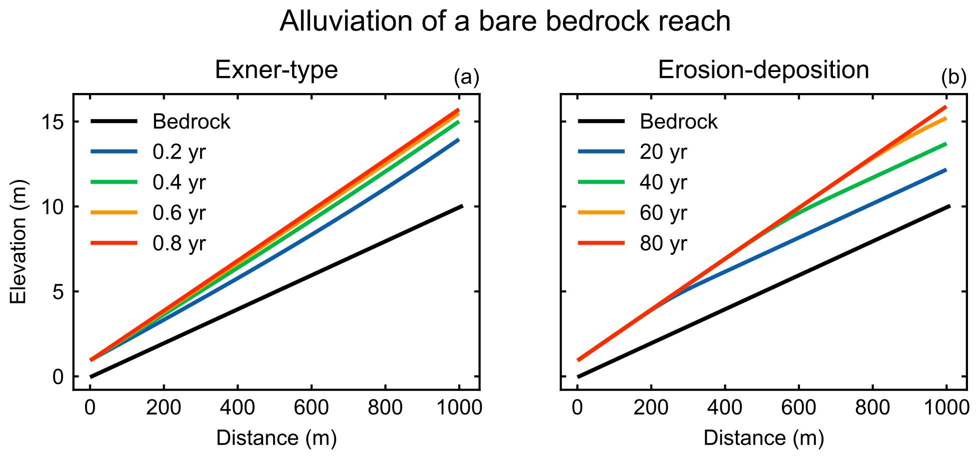

Alluviation of a bare bedrock reach
Exner-type
(a)
Bedrock
0.2 yr
0.4 yr
0.6 yr
0.8 yr
Elevation (m)
0
5
10
15
0
200
400
600
800
1000
Distance (m)
Erosion-deposition
(b)
Bedrock
20 yr
40 yr
60 yr
80 yr
0
200
400
600
800
1000
Distance (m)

Figure 4.

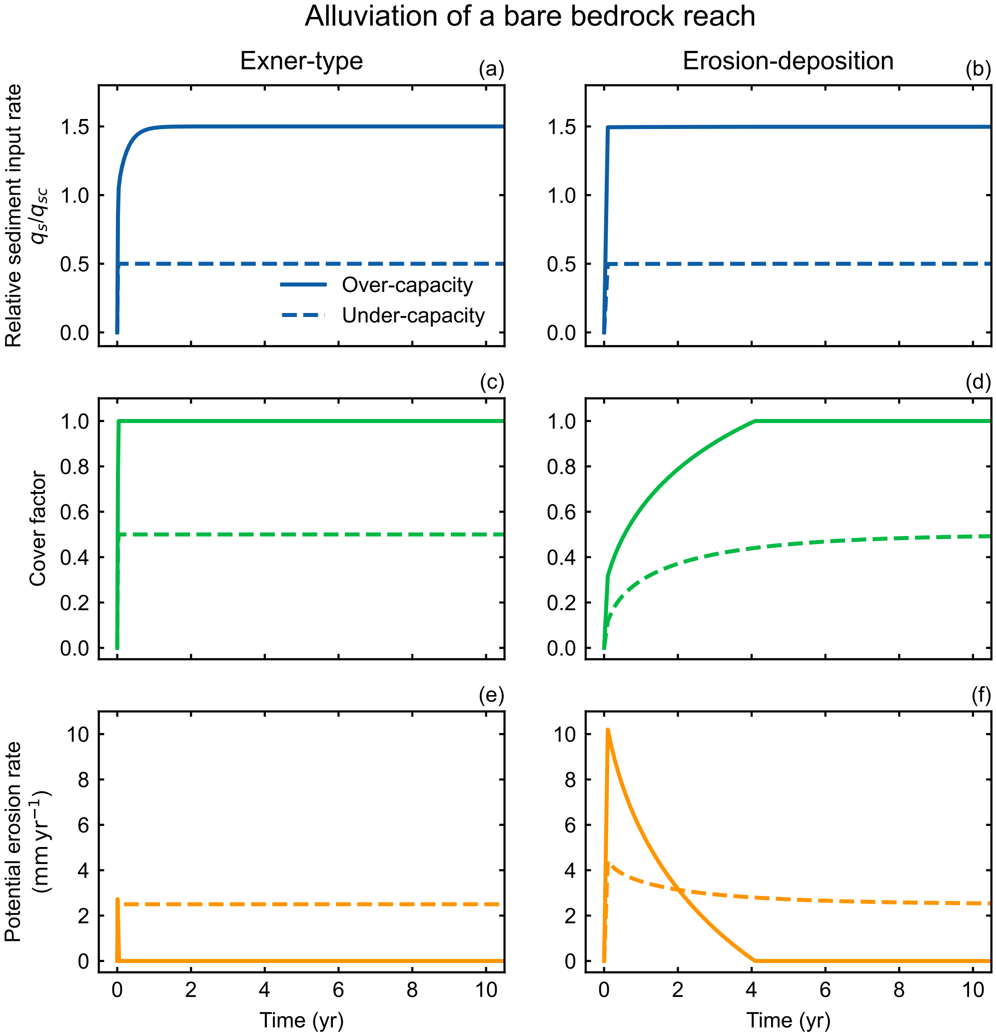

Alluviation of a bare bedrock reach
Exner-type
Erosion-deposition
(a)
(b)
(c)
(d)
(e)
(f)
Relative sediment input rate
q_s/q_{sc}
Over-capacity
Under-capacity
Cover factor
Potential erosion rate
(mm yr^{-1})
Time (yr)

Figure 5.

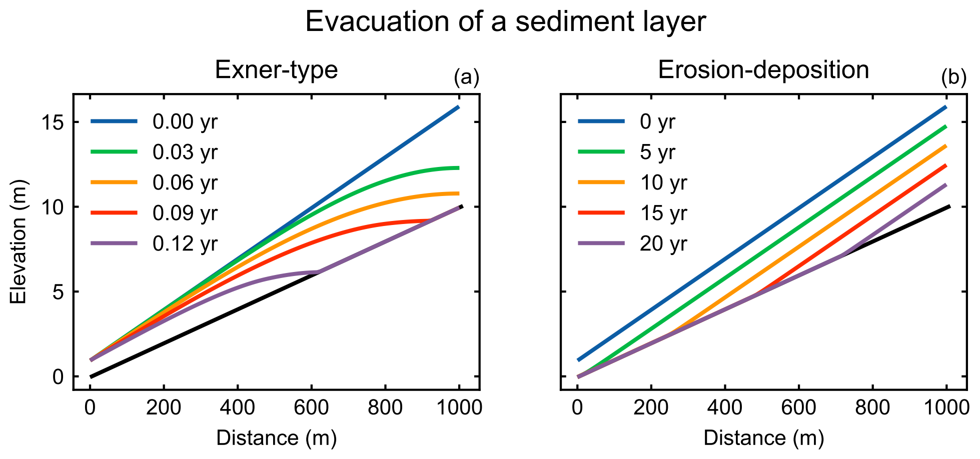

Evacuation of a sediment layer
Exner-type
(a)
0.00 yr
0.03 yr
0.06 yr
0.09 yr
0.12 yr
Elevation (m)
Distance (m)
0
5
10
15
0
200
400
600
800
1000
Erosion-deposition
(b)
0 yr
5 yr
10 yr
15 yr
20 yr
Distance (m)
0
200
400
600
800
1000

Figure 6.

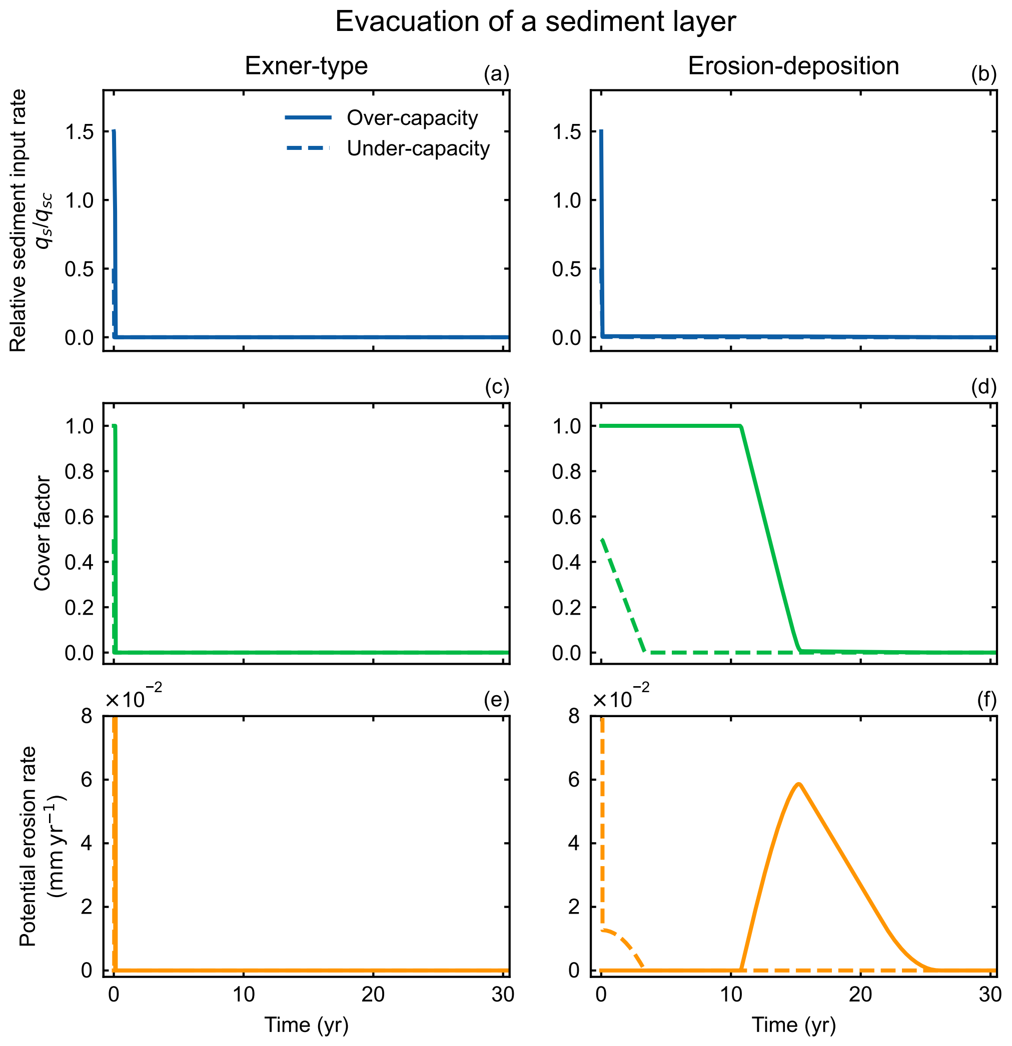

Evacuation of a sediment layer
Exner-type
Erosion-deposition
(a)
(b)
(c)
(d)
(e)
(f)
Over-capacity
Under-capacity
Relative sediment input rate
q_s/q_{sc}
Cover factor
Potential erosion rate
(mm yr^{-1})
$\times 10^{-2}$
Time (yr)

Figure 7.

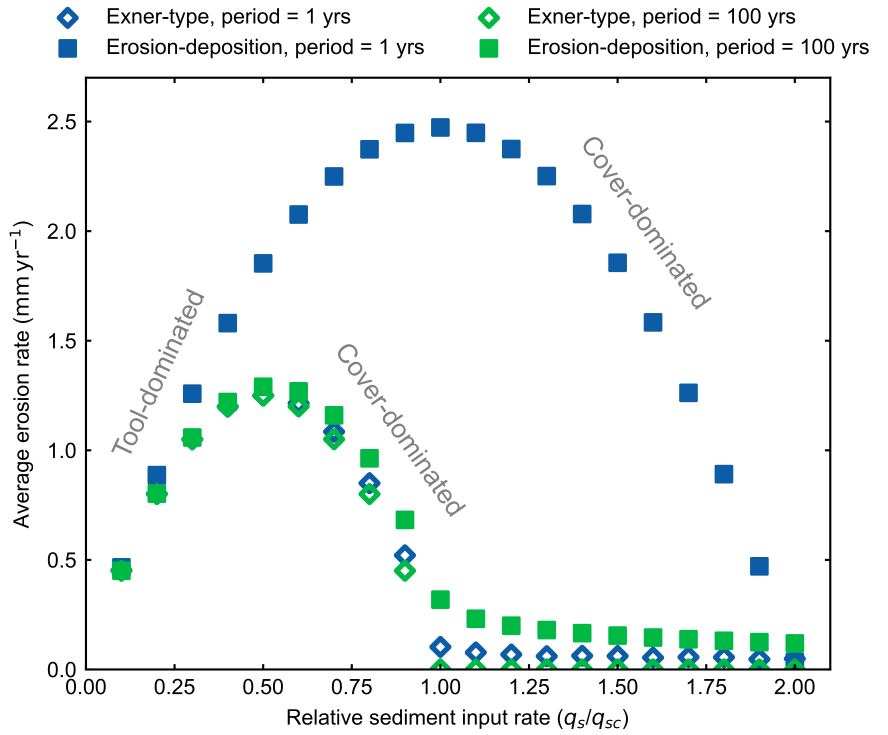
Exner-type, period = 1 yrs
Exner-type, period = 100 yrs
Erosion-deposition, period = 1 yrs
Erosion-deposition, period = 100 yrs
Tool-dominated
Cover-dominated
Cover-dominated
Average erosion rate (mm yr^{-1})
Relative sediment input rate (q_s/q_{sc})
0.0
0.5
1.0
1.5
2.0
2.5
0.00
0.25
0.50
0.75
1.00
1.25
1.50
1.75
2.00

Figure 8.

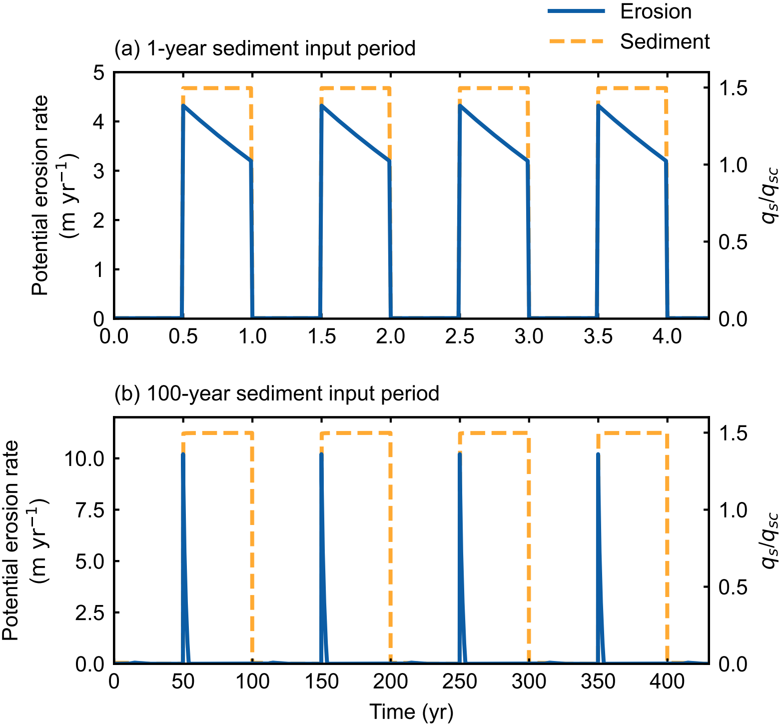

Erosion
Sediment
(a) 1-year sediment input period
Potential erosion rate (m yr^{-1})
q_s/q_{sc}
(b) 100-year sediment input period
Potential erosion rate (m yr^{-1})
q_s/q_{sc}
Time (yr)

Figure 9.

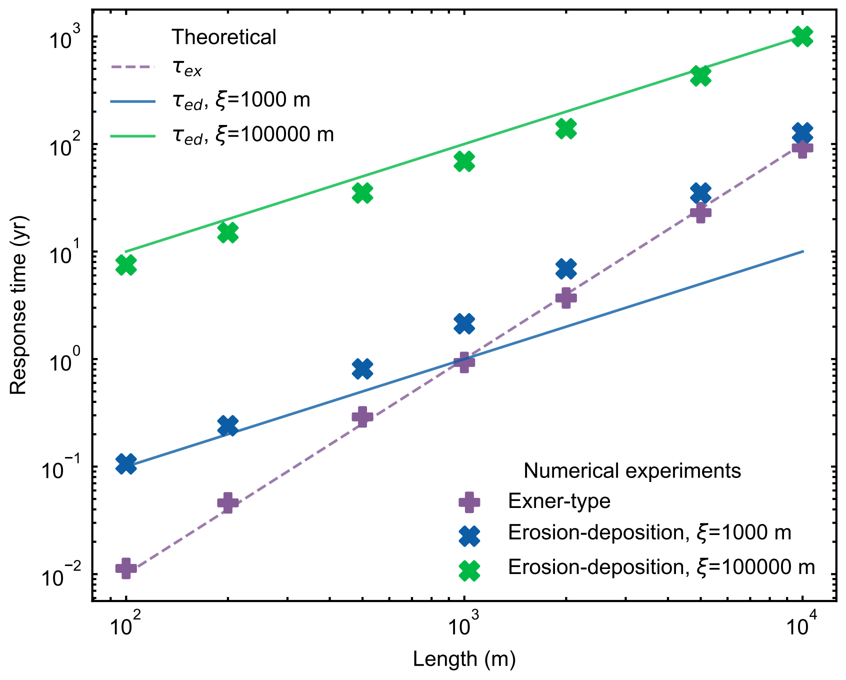

Theoretical
τ_{ex}
τ_{ed}, ξ=1000 m
τ_{ed}, ξ=100000 m
Numerical experiments
Exner-type
Erosion-deposition, ξ=1000 m
Erosion-deposition, ξ=100000 m
Response time (yr)
Length (m)
10^{-2}
10^{-1}
10^{0}
10^{1}
10^{2}
10^{3}
10^{2}
10^{3}
10^{4}